EFDA–JET–PR(12)48

J. Gaspar, J.-L. Gardarein, F. Rigollet, C. Le Niliot, Y. Corre,
S. Devaux and JET EFDA contributors

Nonlinear Heat Flux Estimation in the JET Divertor with the ITER-Like Wall

Nonlinear Heat Flux Estimation in the JET Divertor with the ITER-Like Wall

J. Gaspar[1], J.-L. Gardarein[1], F. Rigollet[1], C. Le Niliot[1], Y. Corre[b], S. Devaux[3] and JET EFDA contributors
and JET EFDA contributors*

JET-EFDA, Culham Science Centre, OX14 3DB, Abingdon, UK

[1]Aix-Marseille University,IUSTI UMR 7343 CNRS, - 5 rue Enrico Fermi - 13453 Marseille - France
[2]CEA, IRFM, Cadarache 13108 Saint Paul lez Durance, France
[3]Max-Planck-Institut fur Plasmaphysik, EURATOM-Association, D-85748 Garching, Germany
** See annex of F. Romanelli et al, "Overview of JET Results",*
(24th IAEA Fusion Energy Conference, San Diego, USA (2012)).

Preprint of Paper to be submitted for publication in
International Journal on Thermal Sciences

ABSTRACT

The present paper deals with a nonlinear unsteady heat flux calculation in the case when measurements are provided by only one thermocouple (TC) embedded in the material and the spatial shape of the unknown surface heat flux is given. This inverse problem is solved with the Conjugate Gradient Method (CGM) combined with the adjoint state, the direct problem being solved with the finite element method. This heat flux estimation technique is illustrated in the case of the plasma facing components located in the JET tokamak divertor that can be exposed to several $MW.m^{-2}$ during more than 10 seconds. In those tiles, few embedded thermocouples (TC) located 1 cm below the tile surface are used to measure the bulk temperatures of the Carbon Fiber Composite (CFC) composite tiles (which are coated with 14μm of tungsten for the International Thermonuclear Experimental Reactor (ITER) like wall). A numerical study is first presented in order to validate the heat flux calculation and to study the accuracy of the method. Then experimental data from a recent shot with the ITER-like wall configuration are used in the heat flux calculation presented here. Results are compared with those obtained with the deconvolution technique in the linear case, on a simplified geometry of the tiles.

1. INTRODUCTION

Internal components of magnetic confinement fusion machines are subjected to significant heat fluxes. As an example, in the Joint European Torus (JET), several MW are injected in the plasma for about 10 seconds [1]. A large part of this power (between 50% and 70%) is directed towards the uncooled Plasma Facing Components (PFC). These components were originally made of Carbon Fiber Composite (CFC) composites. Since 2011, in the ITER-like Wall project, all PFC surfaces are made of metallic materials: a part of the divertor CFC tiles (numbered 1,3,4,6,7,8) have been covered with a tungsten deposit of about 14μm [2, 3], tiles n°5 are made of bulk tungsten [4] and the upper part of the machine is coated with a beryllium deposit. In JET experiments, for better understanding and control the heat transfer from the plasma to the surrounding wall, it is important to measure the surface temperature of the PFC and to estimate the imposed surface heat flux. An infrared system and several embedded thermocouples are used to measure respectively the surface and bulk temperatures of the PFC [5].

Concerning the heat flux estimations, several methods have been developed in the past using only the IR data [6] or both TC and IR data [7] on CFC tiles. In [7], the thermocouple (only one sensitive TC per CFC tile) was used to estimate the heat flux with a deconvolution method associated to a regularization procedure. Since the heat flux depends both on time and space, the TC measurement was not sufficient to find both time and space heat flux dependencies. So, the heat flux spatial shape was fixed after an analysis of IR data. Computation of heat flux was done in a direct way, just applying the IR data as Dirichlet's conditions. The comparisons between the two estimated heat fluxes (with TC and with IR) showed a good agreement on the CFC tiles with 'clean' surfaces but a poor agreement on tiles having an unknown carbon layer poorly attached to its surface, coming

from erosion of CFC tiles elsewhere in the Tokamak. The correct heat flux on that 'non-clean' tiles was estimated with the embedded TC because it has been demonstrated that it was not sensitive to the surface carbon layer properties. Only the heat flux spatial shape had to be known. Another advantage of the deconvolution method is its fast computing ability. This is due first to the simplified tile geometry used by the thermal quadrupoles modelling [8]. This fast computing is also due to the linear system theory inherent to the deconvolution method: thermophysical properties are supposed constant with temperature. Then, heat flux estimations are typically done is less than one minute with an error less than 20%.

In the metallic environment of the ITER-like wall tiles, IR thermography, which remains undeniably the major system to monitor the surface temperature of the plasma facing components, becomes more challenging than carbon environment due to low emissivities (0.2 for Beryllium and 0.4 for tungsten) and then high reflection issues. Parallel work is done to develop temperature measurement devices of such metallic surfaces using the active pyrometry principle [9, 10]. Without such advanced thermographic measurement, heat flux estimation has to be done only with the thermocouples measurements but its spatial shape cannot be estimated with IR data anymore because of the multiple reflections. This heat flux spatial profile will then be given by a heuristic formulation depending on the plasma parameters proposed by [11].

The present paper proposed an alternative method to the deconvolution of TC measurements. It is an inverse thermal calculation based on Conjugate Gradients Method (CGM) used to deduce the deposited heat flux without use of IR measurements. The variations of the thermal properties with temperature are taken into account and the exact geometry of the tile is modelled using finite elements nodes in two dimensions (CAST3M software). The first part of this paper is devoted to the description of the experimental set-up, including the JET Tokamak, the materials, the geometry of the tiles and the studied shot. The second part is dedicated to the presentation of the heat flux estimation, for the divertor tiles of the JET tokamak, by the Conjugate Gradient Method (CGM) with the adjoint state. In the third part, numerical data are used for a sensitivity analysis in order to show that the thermocouple measurements are not sensitive to the tungsten layer deposited on the surface and that this layer can be neglected. Uncertainties on the estimated heat flux are also investigated in this part with the numerical data. Finally, we present experimental results of heat flux computation on 2 tiles of the divertor during a shot with Neutral Beam Injector (NBI) heating, performed in March 2012. Results will be compared with those obtained with the deconvolution technique [12] in the linear case, on a simplified geometry of the tiles.

2. DESCRIPTION OF THE EXPERIMENTAL SET-UP

The Joint European Torus, based at Culham in Great Britain is a large Tokamak (major radius torus: R = 3m, minor radius: r = 0.9m) with a divertor at the bottom of the vacuum vessel. The divertor function is to modify magnetic field lines in the plasma boundary region to conduct both particles and heat fluxes emerging from the plasma to the divertor volume which is separated from the main

plasma volume. The main interaction between plasma and wall takes place in the divertor. It is designed for improved particle and heat exhaust and reduced pollution of the main plasma. The JET divertor is symmetric around the torus principal axis and is localized at the bottom of the tokamak (Fig.(1)). The divertor function is controlled by a set of dedicated poloïdal magnetic coils in the divertor volume. Carbon tiles covered with tungsten deposit constitute the target of the particle and heat fluxes that follow the magnetic lines. For the duration of the high power pulses they rely basically on passive cooling only. The temperature rise limits the duration of high power pulses to about 10 secs. The deposited heat flux is slowly transferred to the divertor cooling system between the pulses. It is precisely on these target tiles that the heat flux is maximum.

In JET, some plasma facing components are tile-like structures (Fig.(1) and (2)) made of Carbon Fiber Composite (CFC) coated with a tungsten deposit of about 14μm. The thermal properties of the composite are presented in Fig.(3) in the weave plane of the CFC (depth and toroidal directions for the vertical tiles), constituted by the z and y directions in Fig.(1) [5]. The thermal conductivity in the poloïdal direction x is about a factor 4 lower for the vertical tiles (so $\lambda_y = \lambda_z$ and $\lambda_x \approx \lambda_z/4$). The density does not depend on the temperature and is equal to 1820kg.m^{-3}. Two internal temperatures are measured by two type K thermocouples (Fig.(1)) with acquisition time step of 20ms. The tile studied in this paper and the thermocouple location are also presented in Fig.(2). In all calculations, x represents the poloïdal direction, y the toroïdal direction and z the depth in the tile. The tiles are mounted onto the tile carriers with a dumbbell fixation and the back of tiles are in contact with the carrier only in discrete locations. Moreover, the JET chamber is under high vacuum condition during operation.

3. CONJUGATE GRADIENTS METHOD WITH THE ADJOINT PROBLEM

The direct heat conduction problems are concerned with the determination of temperature at interior points of a region when the initial and boundary conditions, thermophysical properties and heat sourced or flux are specified. In contrast, the inverse heat conduction problem involves the determination of the surface conditions [13, 14, 15, 16, 17, 18, 19], energy generation [16, 20] and thermophysical properties [20, 21, 22, 23] from the knowledge of temperature measurements taken at several points in the body or at the boundaries. The solution of inverse problems is much more difficult in comparison with direct problems due to instability in solution: thus, they are called ill-posed problems. One application among these inverse problems is heat flux estimation from boundary conditions [14, 15, 18, 19]. To solve these inverse problems, different inverse methods have been developed over the years [24]. One of these methods known for its robustness and accuracy is the Conjugate Gradient Method (CGM) with the adjoint problem. The CGM is an iterative method of minimization of gradient type which allows accurate estimation of surface heat flux, thanks to an accurate modelling of heat exchanges. The CGM is also called an iterative regularization method, which means the regularization procedure is performed during the iterative processes and thus the determination of optimal regularization conditions is controlled by the choice of the stopping criterion.

The stopping criterion will be defined by the discrepancy principle to stop the iterations at the optimal step [24, 25]. The bases of the method are written in [13, 26]. The particularity of the CGM comes from that the directions of descent of each iteration are conjugated with the preceding one, through a conjugation coefficient. Several conjugation coefficients are introduced in the literature with different performances [27]. Here in addition of the CGM we use the adjoint problem. This problem results in an expression for the gradient direction involving a Lagrange Multiplier. It prevents from the computation of the sensitivity matrix, which is a time-consuming process when the number of values to be estimated becomes large. This property enables the estimation of a large number of values especially in nonlinear problems as presented here.

3.1. DIRECT FORMULATION

On the tiles of the divertor JET, the heat flux depends mainly on the x location and it is deposited directly at the surface Γ_2. Furthermore the heat flux presents a symmetry in the toroïdal direction (y-direction in Fig.(1)). This direction will therefore be neglected in modeling, the problem is then bi-dimensional in x and z (see Fig.(2)). The mathematical formulation of this unsteady heat conduction problem is given as follows (for clarity we note T = T(x, z, t):

$$p(x,t) = \varphi(x,t) \tag{1a}$$

$$\rho Cp(T)\frac{\partial T}{\partial t} - \vec{\nabla}.\left(\lambda(T)\vec{\nabla}(T)\right) = 0 \quad in\ \Omega \tag{1b}$$

$$-\lambda(T)\frac{\partial T}{\partial n_1} = \varepsilon_{cfc}\,\sigma(T^4 - T_{amb}^4) \quad on\ \Gamma_1 \tag{1c}$$

$$-\lambda(T)\frac{\partial T}{\partial n_2} = \varepsilon_w\sigma(T^4 - T_{amb}^4) - \varphi(x,t) \quad on\ \Gamma_2 \tag{1d}$$

This mathematical formulation is solved by the finite element method with the software CAST3M [28]. The geometry is composed by 628 elements, the elements are quadratic with 4 nodes. These direct calculations enable to compute the unsteady temperature field T(x, z, t) in the tile, particularly at the TC location.

3.2. INVERSE PROBLEM

We denote p, the function to be determined, in our case this function is the heat flux $\phi(x, t)$ of the tile surface:

$$T = T_0 \quad at\ t=0 \tag{2}$$

The objective of the inverse analysis is to determine the unknown time evolution of the heat flux given the unsteady embedded measurement at the TC location. We note Y (x_s, z_s, t) the temperature

data taken over time by a thermocouple in the CFC (see Fig.(2)). The solution of the direct problem Eqs.(1) obtained for the given function p is noted T(x, z, t; p). The inverse heat conduction problem consists in the determination of p(x, t) such as ||T(x_s, z_s, t; p) – Y (x_s, z_s, t)k is minimal. For this, we define the cost function which is the following quadratic criterion measuring the Euclidean distances between the experimental data and the model.

$$J(p) = \frac{1}{2}\int_0^{t_f} \left(T(x_s, z_s, t; p) - Y(x_s, z_s, t)\right)^2 dt \tag{3}$$

with T(x_s, z_s, t; p) the temperature at the TC location in the CFC calculated with the function p.

The Conjugate Gradient Method is the iterative process used to estimate the function p by minimizing the cost function J(p). The CGM calculates the new iterate p^{n+1} from the previous iteration p^n (with n the iteration number), by:

$$p^{n+1} = p^n - \gamma^n d^n \tag{4}$$

where γ^n is the step size, determined by the resolution of the sensitivity problem (see part 3.3), and dn is the direction of descent given by [13, 26]:

$$d^n = \begin{cases} \nabla J(p^n) & if\ n = 0 \\ \nabla J(p^n) + \beta^n d^{n-1} & if\ n > 1 \end{cases} \tag{5}$$

where $\nabla J(p^n)$ is the gradient of the cost function, determined by the resolution of the adjoint problem (see part 3.4). At the first iteration (n = 0), the steepest method is applied, the direction of descent is equal to the gradient of the cost function $\nabla J(p^n)$. Thereafter the direction of descent d^n is conjugated to the previous one d^{n-1} with the conjugate coefficient βn. In the literature, different versions of the CGM can be found, depending on how the conjugation coefficients are computed. In this study we use the Polak-Ribière-Polyak's version of the CGM, the conjugate coefficient is computed as [29, 30]:

$$\beta^n = \frac{\int \left[\nabla J(p^n)\left(\nabla J(p^n) - \nabla J(p^{n-1})\right)\right] dt}{\|\nabla J(p^{n-1})\|^2} \tag{6}$$

3.3. SENSITIVITY PROBLEM AND SEARCH STEP SIZE

The sensitivity function δT(x, z, t) describes the temperature rise resulting from of a variation of function of ηδp, the sensitivity function is defined by [13, 26]:

$$\delta T(x, z, t) = lim_{\eta \to 0} \frac{T(x, z, t; p + \eta\delta p) - T(x, z, t; p)}{\eta} \tag{7}$$

To determine the sensitivity problem that defines the sensitivity function,the direct problem Eqs.(1) is written first for p, then for p + δp. The results are substrated, and we apply the Eq.(7). Finally we get the system describing the evolution of the sensitivity function (for clarity we note δT = δT(x, z, t)):

$$\frac{\partial[\rho Cp(T)\delta T]}{\partial t} - \vec{\nabla}.\left(\lambda(T)\vec{\nabla}(\delta T)\right) = 0 \quad in\ \Omega \tag{8a}$$

$$-\frac{\partial[\lambda(T)\delta T]}{\partial n_1} = \left[4\varepsilon_{cfc}\,\sigma T^3\right]\delta T \quad on\ \Gamma_1 \tag{8b}$$

$$-\frac{\partial[\lambda(T)\delta T]}{\partial n_2} = \left[4\varepsilon_w \sigma T^3\right]\delta T - \delta p \quad on\ \Gamma_2 \tag{8c}$$

$$\delta T = 0 \quad at\ t=0 \tag{8d}$$

The coefficient γ^n, which determines the step size between the iterate pn and p^{n+1} Eq.(4), is obtained by minimizing $J(p^{n+1})$ with respect to γ^n:

$$J(p^{n+1}) = \frac{1}{2}\int_0^{t_f} \left(T(x_s, z_s, t; p^n - \gamma^n d^n) - Y(x_s, z_s, t)\right)^2 dt \tag{9}$$

To calculate the minimum of $J(p^{n+1})$, a linearization of $T(x_s, z_s, t; p^n - \gamma^n d^n)$ is carried out:

$$T(x_s, z_s, t; p^n - \gamma^n d^n) \approx T(x_s, z_s, t; p^n) - \gamma^n \delta T(x_s, z_s, t; d^n) \tag{10}$$

Then Eq.(10) is applied in Eq.(9) and after rearrangement, the following expression is obtained for step size γ^n:

$$\gamma^n = \frac{\int_0^{t_f} \left(T(x_s, z_s, t) - Y(x_s, z_s, t)\right)\delta T(x_s, z_s, t)dt}{\int_0^{t_f} \left(\delta T(x_s, z_s, t)\right)^2 dt} \tag{11}$$

3.4. ADJOINT METHOD

The adjoint method is used to calculate the gradient $\nabla J(p)$ of the cost function J(p). For that, the adjoint problem is built by multiplying the equations (1) (of Ω domains) by the Lagrange multipliers (or adjoint function) ψ. Then, the results are integrated over time and space. The results are added to the cost function Eq.(4), and finally the expression of the Lagrangian is [13, 24, 26]:

$$L(T, \psi, p) = J(p) + \int_0^{t_f}\int_\Omega \left(\rho Cp(T)\frac{\partial T}{\partial t} - \Delta(\lambda(T)T) = 0\right)\psi d\Omega dt \tag{12}$$

The directional derivative $D_{\delta p}J(p)$ of Eq.(12) is obtained by the variational principle and by using the definition of the sensitivity function:

$$\begin{aligned} &D_{\delta p}J(p) = \\ &\int_0^{t_f} \left(T(x_s, z_s, t; p) - Y(x_s, z_s, t)\right)\delta T dt \\ &+ \int_0^{t_f}\int_\Omega \left(\frac{\partial \rho Cp(T)\delta T}{\partial t} - \Delta(\lambda(T)\delta T) - \delta p \Delta T\right)\psi d\Omega dt \end{aligned} \tag{13}$$

After integrating by parts with respect to t, using Green's formula and applying the boundary conditions of the sensitivity problem, the equations of the adjoint problem can be written as following (for clarity we note $\psi = \psi(x, z, t)$):

$$\rho Cp(T)\frac{\partial \psi}{\partial t} + \vec{\nabla}.\left(\lambda(T)\vec{\nabla}(\psi)\right) = E \quad in\ \Omega \tag{14a}$$

$$-\lambda(T)\frac{\partial \psi}{\partial n_1} = \left[4\varepsilon_{cfc}\,\sigma T^3\right]\psi \quad on\ \Gamma_1 \tag{14b}$$

$$-\lambda(T)\frac{\partial \psi}{\partial n_1} = \left[4\varepsilon_{w}\,\sigma T^3\right]\psi \quad on\ \Gamma_2 \tag{14c}$$

$$\psi = 0 \quad at\ t = t_f \tag{14d}$$

with the errors terms E defined by:

$$E(x_s, t) = T(x_s, z_s, t; p) - Y(x_s, z_s, t) \tag{15}$$

We note that in the adjoint problem the initial condition is replaced by a final condition at $t = t_f$. The resolution must be done in a retrograde way. Even if the adjoint problem (as the sensitivity problem) is not the direct problem, it can be solved with the same element finite code (CAST3M).

3.5. GRADIENT EQUATION

The expression of the gradient for the cost function J(p) is [14, 15, 18, 19]:

$$\nabla J(p) = \psi(x, z, t) \quad on\ \Gamma_1 \tag{16}$$

We note that $\nabla J(p)$ is always equal to zero for the last time due to the final condition of the adjoint problem. The final time cannot be estimated.

3.6. THE FINITE DIMENSIONAL CASE

The inverse problem introduced up to here does not require any a priori information on the nature of the unknown function to be resolved, this kind of problem is called 'infinite dimensional'. There a priori information is available on the nature of the unknown function p, this one can be written as following [13]:

$$p(x, t) = p(t)\varphi(x) \tag{17}$$

where $\varphi(x)$ is the normalized heat flux spatial shape. In our case the 'a priori' $\varphi(x)$ is given by the heuristic formulation built with IR thermography during Carbon-wall operations [11], defined by:

$$\varphi(x) = \frac{1}{2} exp\left[\left(\frac{x}{2\lambda_q f_x}\right)^2 - \frac{\bar{x}}{\lambda_q f_x}\right] erfc\left(\frac{x}{2\lambda_q f_x} - \frac{\bar{x}}{x}\right) + \varphi_{BG\%} \quad and \quad \bar{x} = x - x_0 \tag{18}$$

where x is the target coordinate, x_0 is the strike line position, f_x is the magnetic flux expansion, λ_q is the power decay length and φBG% is a fixed percentage of the peak heat flux value. All that parameters are supposed known. Fig.(4) shows a representative example of heat flux shape present in the JET tokamak. p(t) is then the peak heat load (in $W.m^{-2}$) on the strike line position whose value is determined at each time. in that 'finite dimensionnal' case, the only change in the methodology for solving the inverse problem is the computation of the gradient defined by Eq.(16). When p is given by Eq.(17) the gradient and the sensitivity function is computed as follows:

$$\nabla J(x,t) = \nabla J(t)\varphi(x) \tag{19}$$

$$\delta T(x,t) = \delta T(t)\varphi(x) \tag{20}$$

3.7. STOPPING CRITERION

The conjugate gradient method is also called as an iterative regularization method, in this kind of method the regularization is provided by the choice of the stopping criterion. If the measurements have no errors, the traditional stopping criterion is written as following:

$$J(p^{n+1}) \leq \epsilon \tag{21}$$

where ∈ is a small specified number. In fact, temperature data contain measurement errors, then the stopping criterion to use is given by the discrepancy principle [24, 25]. By assuming that the estimation is optimal when measurements and model differ only by the noise measurement (of standard deviation σnoise), the discrepancy principle establishes the threshold value of the cost function with the Eq.(5) by:

$$J_{threshold} = \frac{1}{2}\int_0^{t_f} (\sigma_{noise})^2 \, dt \tag{22}$$

3.8. Summary of computational procedure

The computational procedure for the resolution of this inverse problem is:

- STEP 1: Choose an initial guess p_0 (usually $p_0 = 0$) set $n = 0$.
- STEP 2: Solve the direct problem given by Eqs.(1).
- STEP 3: Calculate the cost function by Eq.(3) and compare to the stopping criterion Eq.(22), continue if not satisfied.
- STEP 4: Calculate the vector errors by Eq.(15), solve the adjoint problem given by Eqs.(14).
- STEP 5: Calculate the gradient of the cost function $\nabla J(p^n)$ from Eq.(16).

- STEP 6: Calculate the conjugate coefficient βn and the direction of descent dn from Eqs.(5)-(6).
- STEP 7: Set $\delta p = d^n$, and solve the sensitivity problem given by Eqs.(8).
- STEP 8: Calculate the step size γn from Eq.(11).
- STEP 9: Calculate the new iterate p^{n+1} from Eq.(4) and return to STEP 2.

4. NUMERICAL STUDY

4.1. NUMERICAL VALIDATION AND CHOICE OF THE TUNGSTEN (W) DEPOSIT MODELLING

JET is currently running experiments with the ITER-like wall (ILW), beryllium in the main chamber and tungsten for the divertor target plates (including a bulk tungsten divertor row for the central horizontal target and W-coated CFC for the vertical tiles). Surface temperature measurements remains an essential issue to guarantee plasma operation in acceptable temperature range for each material, typically [200°C-1300°C] for tungsten (between brittleness and recrystallisation domains). The tiles 3 and 7 (see Fig.(1)) are made of carbon Dunlop whose thermal properties are describbed on Fig. (3). In the new ITERLike Wall configuration, these tiles have been coated with a 14μm tungsten layer. In this part we study the influence of this thin layer on the measurementstaken by the upper thermocouple located approximately 1 cm below the surface. The method described above is applied on the geometry of the tile 7 with and without the tungsten coating modelling. Three models of the tile are presented:

- pure CFC: the tile 7 made of CFC with a radiative exchange on all boundaries with emissivity equal to $\varepsilon_{cfc} = 0.83$
- CFC with simplified W coating: the tile 7 made of CFC with a radiative exchange on Γ_1 on Γ_2 with emissivities respectively equal to εcfc and $\varepsilon_W = 0.4$
- CFC with W coating: the tile 7 made of CFC with a radiative exchange on Γ_1 with εcfc and the true layer with $\varepsilon_W = 0.4$ on Γ_2 (reference case)

This three models have been tested in a virtual experiment, in which a known heat flux is imposed to simulate noisy measurement. The simulated time is 25s with a time step of $dt = 2.10^{-2}$s, then the estimation is performed on 1251 values. The time evolution of the heat flux used is shown in Fig. (5) by (—) and the shape heat flux is shown in Fig.(4). This heat flux input on the front face Γ_2 of the tile 7, the direct calculation provides the temperature at the TC location Yexact. Then the noisy simulated measurements Y are calculated by:

$$Y = Y_{exact} + \omega\sigma_{noise} \tag{23}$$

σ_{noise} is the standard deviation of the measurement ($\sigma_{noise} = 0.5$K in our virtual experiment), and ω is a random variable with a Gaussian distribution, zero mean and a standard deviation equal to 1. This noisy simulated measurement (shown in Fig.(6) by (—)) are used as input in the CGM method. Even if this can be qualified of 'inverse crime', this step is mandatory to qualify the feasibility of the

chosen method. After that, sensitivity of the method to supposed known parameters (like emissivity ans Strike Point position) will also be presented, still using noisy simulated measurements. The initial guess for the three cases is the same and equal to 0. The stopping criterion, computed with Eq.(22), is reached at the iteration 44 for the first modelling, 45 for the second one and 52 for the reference case (the computational time of a single iteration is about 10 min with a CPU performance of 2.5GHz with 8Mo cache and 20Go of RAM).

To quantify the deviation between the estimated and exact values of p(t) function we introduce the Root-Mean-Square (RMS) error, eRMS defined by :

$$e_{RMS} = \sqrt{\frac{1}{N_m}\sum_{i=1}^{N_m}\left(\varphi_{est}\left(x_s, t_i; p\right) - \varphi_{exa}\left(x_s, t_i\right)\right)^2} \tag{24}$$

where Nm denotes the number of unsteady measurements used in the estimation in $0 \le t \le t_f$, and the subscripts 'est' and 'exa' refer respectively to the estimated and exact heat flux.

Table (1) and Figure (5) present the results of the estimations done with the three modelling previously cited. Tab.(1) shows that the values of the RMS errors is quite the same for each modelling. Fig.(5) presents the time evolution of the estimated heat flux, the three modelling cases, and the exact heat flux. Fig.(5) shows that the estimated heat flux of each modelling are equivalent. Then for the rest of the paper the second modelling corresponding to the real geometry made of CFC, with a radiative exchange treated with ε_{cfc} on Γ_1 and ε_w on Γ_2, will be used. This model is the nearest from the reference case and is the faster one. Furthermore, these results enable to validate numerically the feasibility of solving our inverse problem. Magnitude and time behavior of the surface heat flux are well recovered despite the use of one embedded TC, thanks to the 'a priori' on the spatial distribution of heat flux [11]. Noise on the measurements (with a realistic standard deviation) induces some oscillations around the exact values of the heat flux. The estimation is independent of the initial guess (in our case 0). Even if there are the time of occurrence of the step variations (t = 3s, 10s and 15s) are well recovered, oscillations close to these times that are induced by the estimation of this very high temporal frequencies. We have checked that lower frequencies as the triangle or the ramp (not presented here) are better recovered.

Figure (6) presents the noisy measurements of the TC and the temperature computed with the estimated heat flux. The two evolutions coincide, and the residuals between this two evolutions have the same statistical properties as the noise used to synthetise the measurements, except at t = 10s and 15s corresponding to the step variations which are not exactly recovered.

4.2. UNCERTAINTIES ON THE ESTIMATED FUNCTIONS

4.2.1 Uncertainties in strike point location

The strike line position on target, used to calculate the heat flux shape for the inner and outer side, is given by the magnetic equilibrium with typical uncertainties of ±0.5cm [31] on the vertical tiles. This uncertainty affects the heat flux estimation by changing his shape. To evaluate the errors due

to the uncertainty on the strike point location, the estimation has been done with three positions of the strike point:

- the exact position used to simulate the measurement
- an error of +0.5cm
- an error of –0.5cm

Table (2) and Fig.(7) present the results of the estimations done with the three positions previously cited. Tab.(1) shows that the smallest value of the RMS errors is obviously for the exact position. On the other hand we note that an error of 0.5cm around the exact position increases the RMS error depending on the direction of that error, maximum RMS errors being for an error of –0.5cm on the strike point position. Fig.(7) shows the estimated heat flux for each position. As before it is shown that the exact position provides the best estimation of the exact heat flux. We can notice in Fig.(7) that an error of –0.5cm on the strike point position, leads to an overestimation of the heat flux magnitude about 17%, and a negative heat flux in the cooling phase ($t \geq 15s$) about $0.8MW.m^{-2}$. This negative heat flux is estimated to compensate the overestimated heat flux input during the loading phase. Conversely an error of +0.5cm on the strike point position leads to an underestimation of the heat flux magnitude about 16%, and a positive heat flux in the cooling phase about $0.4MW.m^{-2}$. To understand these results we have to compare the strike point and the TC position. In the numerical test case presented here, the exact position of the strike point is set approximatively 1.5cm under the position of the TC. Thus an error of +0.5cm or –0.5cm gets the strike point respectively closer or distant from the TC position. This explains the over and underestimation of the heat flux magnitude. Another important result is that the dynamics of the heat flux is well recovered for each position.

4.2.2 Uncertainties due to error in the measurement

Noise in experimental data induces error in the heat flux estimation. We introduce a method to evaluate the dispersion of estimations induced by the noise on the data, by the determination of the covariance matrix of the estimated function. The study of the confidence in estimated function takes place when the estimation by the CGM is completed. The CGM, contrary to some other gradient techniques (Gauss Newton, Quasi Newton ...), does not calculate the inverse of Hessian matrix (or even an approximation) at each iteration. This is an advantage for the estimation of a large number of values (1251 in our case), because calculations are easier and the estimation can take few iterations. But the method provides no information on the Hessian, and thus the covariance matrix cannot be directly calculated. Then we introduce the Monte Carlo error propagation method, which uses stochastic simulations, to calculate the confidence associated to the estimated functions [32]. The idea is to simulate l virtual noisy data vectors ($l > 500$) for each pixel and then examine the statistics of the corresponding estimated functions, to finally obtain an approximation of the covariance matrix.

Let $\bar{p}$ be the mean of the l estimated vectors $\hat{p_i}$ ($i = 1, ..., l$), let A be a ($l \times m$) matrix where the

i^{th} row contains the difference between the i^{th} estimated function $\hat{p}_i$ and $\bar{p}$.

$$A_i = \hat{p}_i - \bar{p} \tag{25}$$

Then the approximation of the covariance matrix C (m×m) associated to $\bar{p}$ is given by:

$$C = cov(\bar{p}) = \frac{A^t A}{l} \tag{26}$$

The use of other approach based on the statistical properties of the ordinary least square estimator, using the sensitivity matrix, is impossible in our case due to the strong correlation of the values of the function p.

Figure (8) shows the results of the Monte Carlo method for the estimation of the confidence intervals in the estimated heat flux with noisy numerical data ($\sigma_{noise} = 0.5K$). The 68% confidence intervals are represented by error bars (1 plotted over 30). Each error bar is affected to the average of all estimations (> 500) of the heat flux done by the Monte Carlo method. The comparison between the exact evolution of the heat flux and the average of all estimations done by the Monte Carlo, shows the possible bias in the estimation. In this numerical case the 68% confidence interval is quite constant and equal to 2%, a maximum of 4% is observed for the estimation of the step variation at the time close to the step with a bias. The bias and the increase of the confidence interval at this time, is explained by the fact that the step variation is a very high frequency much higher than the Conjugate Gradient Method can estimate.

5. EXPERIMENTAL RESULTS ON THE PULSE NO: 82641

The inverse heat flux calculation has been applied to 2.2T, 2MA in H-mode Pulse No: 82641 performed with Neutral Beam Injector (NBI) heating (10MW during 4s) and with the strike lines positions on the vertical tiles 3 and 7 (low triangularity vertical tile configuration, see Fig.(1)). The diagnostic set-up is made of four embedded type-K thermocouples (TC) 10mm below the tile surface to measure the bulk temperatures of the inner and outer vertical target plates. For Pulse No: 82641 the Inner and Outer Strike Point (ISP/OSP) positions are given by the magnetic equilibrium: 1.3cm below the upper thermocouple on the inner side and 1.8 cm below upper thermocouple on the outer side. Only the upper thermocouple is used for the heat flux computation on each tile. The thermocouple measurements for the 2 upper thermocouples on tiles 3 and 7 are presented on Fig. (9). For this shot the characteristic parameters of the heat flux shape (Eq.(18)) are: $\lambda_q = 2.5mm$, $S = 1mm$, $f_x = 8$, $\varphi_{BG\%} = 3\%$ (attributed to plasma radiation). With these parameters and the strike lines positions, the heat flux shape in the poloïdal direction on the two tiles are computed and presented on Fig.(10). The initial guess of the functions is set equal to zero and the stopping criterion, calculated with the noise measurements of the upper thermocouples, is reached at the iteration 62 for the inner tile and 57 for the outer tile (the computational time of a single iteration is about 10 min with a CPU

performance of 2.5GHz with 8Mb cache and 20Go of RAM).

Figure (11) shows the estimated heat flux with their 68% confidence intervals. Peak heat loads are found to be $\phi_{ISP} \approx 3.2 MW.m^{-2}$ and $\phi_{OSP} \approx 5 MW.m^{-2}$, with respectively ±5% and ±4% uncertainties due to noise measurement at the inner (ISP) and outer strike point (OSP) during the peak heat loads. The 68% confidence intervals plotted in Fig.(11) evolve with time due to the evolution of the noise measurement during the shot, this time evolution can be seen on Fig.(12). The assymetry observed on the estimated heat flux, between the inner and the outer sides of the divertor is a normal assymetry in this plasma configuration. The shot begins at t = 50s with an ohmic heating until t = 59s. The maximum heat fluxes estimated with the thermocouples between t = 59s and t = 64s correspond to the shooting of Neutral Beam Injector (NBI).

In a previous work, a linear approach was used on a simplified geometry for this shot [12], the results of this method are shown in Fig.(13) and are comparedto the present CGM results. Some differences are observed on the dynamic and the magnitude of the estimated heat fluxes. The maximum deviation on the time behavior for the two estimation methods is 0.5s and 1s respectively for the tiles 7 and 3. Deviations between the linear and non linear approach for the estimation of the peak heat loads are about 5% and 10% respectively for the tile 7 and 3. These differences are induced by the variation of the thermal properties with the temperature during the shot and the simplified geometry used in the linear approach. Even if those differences are relatively small in that example, they demonstrate the capability of the present method to take into account a complex geometry and thermophysical properties varying with temperature. These effects will increase significantly for shots involving higher temperature rises and for estimation on other PFC with complex geometry (ITER, DEMO).

CONCLUSION

In this paper, nonlinear unsteady calculations are used with the Conjugate Gradient Method and the adjoint state, for the heat flux estimation on the divertor tiles of the JET tokamak. The inverse approach is applied on the divertor tiles, in the ITER-Like Wall configuration (Carbon tile coated with about 14μm of tungsten). The combination of the heuristic target heat load profiles [11] (mainly constructed with IR thermography during Carbon-wall operation period) with an inverse heat flux calculation using embedded TC data, provides a new way to estimate heat flux on divertor tiles. It should be noted that no a priori information on the time evolution of the heat flux is needed for the estimation. The method is robust in terms of initial guess, typically the initial guess is set to 0 with no influence on the computational time of the estimation.

The numerical feasibility of the inverse problem has been firstly introduced with a modelling study of the divertor tiles in the ITER like wall configuration. The modelling study demonstrated that the tungsten layer on CFC tiles can be modeled by simply modifing the surface emissivity, the tungsten layer has no conductive influence. Uncertainties on the estimated heat flux due to error in the location of the strike point have been estimated with numerical data. We have introduced

the Monte Carlo error propagation method to evaluate the dispersion of estimations induced by the noise measurement, this method determines an approximation of the covariance matrix of the estimated heat flux. Finally the CGM method with the adjoint state is applied on experimental data from the Pulse No: 82641. The first application to JET data with the ITER like wall configuration shows satisfactory results.

The next step could be the improvement of this method to take into account the potential movement of the strike line position during the shot. Moreover, with another direct computation using the heat flux shape and the estimated heat flux, the surface temperatures can be estimated and compared to the other diagnostics in the machine (several IR cameras).

ACKNOWLEDGMENT

This work was supported by EURATOM and carried out within the framework of the European Fusion Development Agreement. The views and opinions expressed herein do not necessarily reflect those of the European Commission.

REFERENCES

[1]. L.D. Horton, et al., Studies in JET divertors of varied geometry. I: Nonseeded plasma operation, Nuclear Fusion **39** (1) (1999).

[2]. H. Maier, R. Neu, H. Greuner, Ch. Hopf, G.F. Matthews, G. Piazza, T. Hirai, G. Counsell, X. Courtois, R. Mitteau, E. Gauthier, J. Likonen, G. Maddaluno, V. Philipps, B. Riccardi, C. Ruset, Tungsten coatings for the 21 JET ITER-like wall project, Journal of Nuclear Materials **363–365** (2007) 1246-1250.

[3]. G.F. Matthews, P. Coad, H. Greuner, M. Hill, T. Hirai, J. Likonen, H. Maier, M. Mayer, R. Neu, V. Philipps, R. Pitts, V. Riccardo, Development of divertor tungsten coatings for the JET ITER-like wall, Journal of Nuclear Materials **390-391** (2009) 934-937.

[4]. Ph. Mertens, H. Altmann, T. Hirai, M. Knaup, O. Neubauer, V. Philipps, J. Rapp, V. Riccardo, S. Sadakov, B. Schweer, A. Terra, I. Uytdenhouwen, U. Samm, A bulk tungsten divertor row for the outer strike point in JET, Journal of Nuclear Materials **84** (2009) 1289-1293.

[5]. V. Ricardo, W. Fundamenski, G.-F. Matthews, Reconstruction of power deposition profiles using JETMkIIGB thermocouple data for ELMy Hmode plasmas, Plasma Physics and Control Fusion **43** (2001) 881-906.

[6]. T. Eich, P. Andrew, A. Hermann, W. Fundamenski, A. Loarte, R.A. Pitts, JET-EFDA contributors, ELM resolved energy distribution studies in the MKII gas-box divertor using infrared thermography, Plasma Physics and Control Fusion **49** (2007) 573-604.

[7]. J-L. Gardarein, Y. Corre, F. rigollet, C. Le Niliot, P. Andrew, Thermal Quadrupoles approach for two-dimensional heat flux Estimation using infrared and thermocouple measurements on the JET tokamak, Int. Journal of Thermal Sciences **48** (2009) 1-13.

[8]. D. Maillet, S. André, J-C Batsale, A. Degiovanni, C. Moyne, Thermal quadrupoles, Wiley & Sons (2000).

[9]. Th. Loarer, F. Brygo, E. Gauthier, C. Grisolia, F. Le Guern, F. Moreau, A. Murari, H. Roche, A. Semerok, Surface temperature measurements by means of pulsed photothermal effects in fusion devices, Journal of Nuclear Materials **363–365** (2007) 1450-1456.

[10]. S. Amiel, T. Loarer, C. Pocheau, H. Roche, M.H. Aumenier, E. Gauthier, C. Le Niliot, F. Rigollet, Surface temperature measurements of plasma facing components with active pyrometry, Journal of Physics: Conference Series **395** (2012) 012074.

[11]. T. Eich, B. Sieglin, A. Scarabosio, W. Fundamenski, R.J. Goldston, A. Herrmann, Inter-ELM Power Decay Length for JET and ASDEX Upgrade: Measurement and Comparison with Heuristic Drift-Based Model, Physical Review Letters **107** (2011) 2150001.

[12]. J-L. Gardarein, J. Gaspar, F. Rigollet, Y. Corre, S. Devaux, Gilles Arnoux, C. Le Niliot, Inversion Heat Conduction Problem using Thermocouple deconvolution: Application to the heat flux estimation in a tokamak, Inverse Problems in Science and Engineering (submitted).

[13]. Y. Jarny, M.N. Ozisik, J.P. Bardon, A general optimization method using adjoint equation for solving multidimensional inverse heat conduction, International Journal of Heat and Mass Transfer **34** (1991) 2911-2919.

[14]. C.H. Huang, S.P.Wang, A three-dimensional inverse heat conduction problem in estimating surface heat flux by conjugate gradient method, International Journal of Heat and Mass Transfer **42** (1999) 3387-3403

[15]. M. Maniana, A. Azima, H. Rhanima, P. Archambault, Problème inverse pour le traitement laser des métaux à transformations de phases, International Journal of Heat and Mass Transfer **48** (2009) 795-804

[16]. R. Abou khachfe, Y. Jarny, Determination of heat sources and heat transfer coefficient for two-dimensional heat flow - numerical and experimental study, International Journal of Heat and Mass Transfer **44** (2001) 1309-1322

[17]. M.J. Colaco, H.R.B. Orlande, Comparison of different versions of the conjugate gradient method of function estimation, Numerical heat transfer part A-Applications **36** (1999) pp. 229–249.

[18]. M. Mohammadiun, A.B. Rahimi, I. Khazaee, Estimation of the timedependent heat flux using the temperature distribution at a point by conjugate gradient method, International Journal of Thermal Sciences **50** (2011) 2443-2450.

[19]. J. Zhou, Y. Zhang, J.K. Chen, Z.C. Feng, Inverse estimation of front surface temperature of a plate with laser heating and convection-radiation cooling, International Journal of Thermal Sciences **52** (2012) 22-30.

[20]. F.A Rodrigues, H.R.B Orlande, G.S Dulikravich,Simultaneous estimation of spatially dependent diffusion coefficient and source term in a nonlinear 1D diffusion problem, Mathematics and Computers in Simulation **66** (2004) 409 - 424.

[21]. C.H. Huang, J.Y. Yan, An inverse problem in simultaneously measuring temperature dependent thermal conductivity and heat capacity, International Journal of Heat and Mass Transfer **38** (1995) 3433-3441

[22]. C.H. Huang, S.C. Chin, A two-dimensional inverse problem in imaging the thermal conductivity of a non-homogeneous medium, International Journal of Heat and Mass Transfer **43** (2000) 4061-4071

[23]. R. Le Goff, D. Delaunay, N. Boyard, Y. Jarny, T. Jurkowski, R. Deterre, On-line temperature measurements for polymer thermal conductivity estimation under injection molding conditions, International Journal of Heat and Mass Transfer **52** (2009) 1443-1450

[24]. O.M. Alifanov, Inverse heat transfer problems, New York Springer-Verlag (1994).

[25]. O.M. Alifanov, E.A. Artyukhin,Regularized numerical solution of nonlinear inverse heat-conduction problem, Journal of Engineering Physics and Thermophysics **29** (1975) 934–938.

[26]. M.N. Ozisik, H.R.B. Orlande, Inverse heat transfer: Fundamentals and applications, New York Taylor & Francis (2000).

[27]. Z.J. Shi, J. Guob, A new family of conjugate gradient methods, Journal of Computational and Applied Mathematics **224** (2009) 444-457

[28]. P. Verpaux, A. Millard, A. Hoffman, L. Ebersolt, CASTEM2000: a modern approach of computerised structural analysis, in: Proceedings of the Recent Advances in Design Procedures for high Temperature Plant, Risley (1988).

[29]. E. Polak, G. Ribiere, Note sur la convergence de méthodes de directions conjuguées, Rev. Francaise Infomat Recherche Operatonelle **3** (1969) 35–43.

[30]. B.T. Polyak, The conjugate gradient method in extremal problems, USSR Computational Mathematics and Mathematical Physics **9** (1969) 94–112.

[31]. Y. Corre,J-L. Gardarein, J. Gaspar, F. Rigollet, G. Arnoux, S. Devaux, T. Eich, C. Giroud, F. Marcotte, B. Sieglin and JET EFDA Contributors, Heat flux calculation using embedded thermocouple in W-coated CFC tiles in the JET tokamak, 39th EPS Conference on Plasma Physics, Stockholm, Sweden (2012).

[32]. R.C. Aster, B. Borchers, C.H. Thurber, Parameter Estimation and Inverse Problems, 1st Edition, Elsevier Academic Press (2005).

Nomenclature

Roman letters

C	*approximation of the covariance matrix*
Cp	*specific heat capacity,* $J.kg^{-1}.K^{-1}$
d^n	*direction of descent at iteration n*
dt	*time step, s*
$D_{\delta p}$	*directional derivative of J at* δp
E	*error term, K*
f_x	*magnetix flux expansion*
$J(p)$	*cost function,* K^2
L	*Lagrangian*
n	*number of current iteration*
n_i	*outward drawn normal to the boundary surface* Γ_i
p	*unknown function*
$\hat{p}$	*estimated function*
$\overline{p}$	*mean of the estimated function*
t	*time, s*
t_f	*final time, s*
T	*temperature, K*
δT	*sensitivity function, K*
x_0	*strike line position, m*
x_s	*poloidal thermocouple position*
x	*poloidal direction, m*
y	*toroidal direction, m*
Y	*measurements, K*
z_s	*radial thermocouple position, m*
z	*radial direction, m*

Greek symbols

λ	*thermal conductivity,* $W.m^{-1}.K^{-1}$
λ_q	*power decay lenght, m*
ρ	*density,* $kg.m^{-3}$
φ	*surface heat flux,* $W.m^{-2}$
Ω	*space domain*
Γ	*boundary surface*
ε	*emissivity*
σ	*Stefan-Boltzmann constant,* $W.m^{-2}.K^{-4}$
ψ	*Lagrange multiplier*
γ	*step size*
φ	*function of space*
β	*conjugation coefficient*
ω	*random variable*
σ_{noise}	*standard deviation of the measurement, K*
∇	*gradient operator*
Δ	*Laplace operator*

Abbreviation

BG	*Background*
CFC	*CarbonFiberComposite*
CGM	*ConjugateGradientMethod*
ILW	*ITERLikeWall*
ISP	*InnerStrikePoint*
NBI	*NeutralBeamInjector*
OSP	*OuterStrikePoint*
RMS	*RootMeanSquare*
W	*Tungsten*

Modelling	e_{RMS} (MW/m^2)	*Iteration*
pure CFC	*0.2633*	*44*
CFC with simplified W coating	*0.2636*	*45*
CFC with W layer	*0.2640*	*52*

Table 1: RMS errors of the estimated heat flux for the three tiles modelling

Position	e_{RMS} $(MW.m^{-2})$	*Iteration*
Exact	*0.26*	*45*
$+0.5cm$	*0.46*	*47*
$-0.5cm$	*0.60*	*52*

Table 2: RMS errors on the estimated values depending on the strike point location.

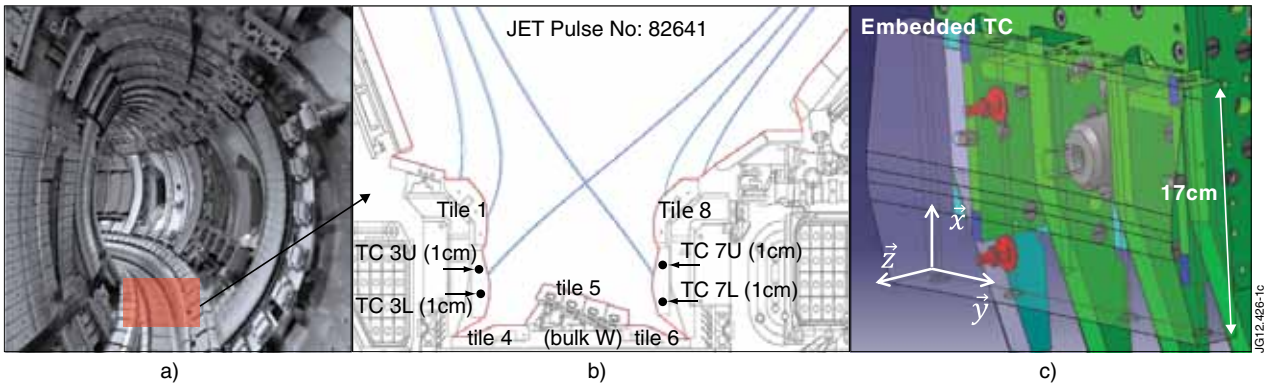

Figure 1: a) Visible picture of the JET chamber with the Iter like wall; b) Poloidal crosssection of the divertor with the magnetic equilibrium of the low triangularity vertical tile configuration. Position of the TC's in the inner (tile 3) and outer (tile 7) target are shown; c) View of the outer vertical tile with upper and lower embedded TC.

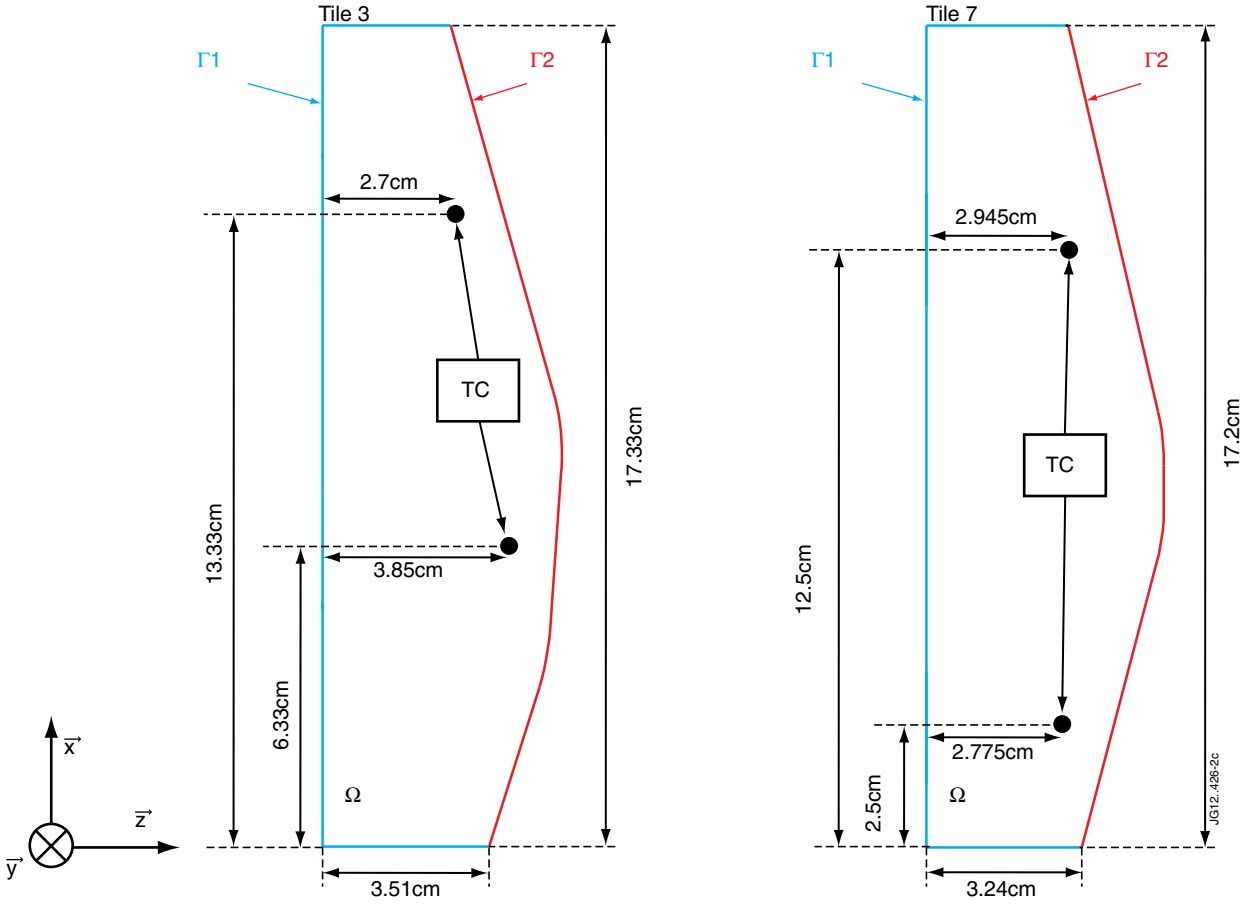

Figure 2: Geometry and dimension of the inner (tile 3) and outer (tile 7) tiles.

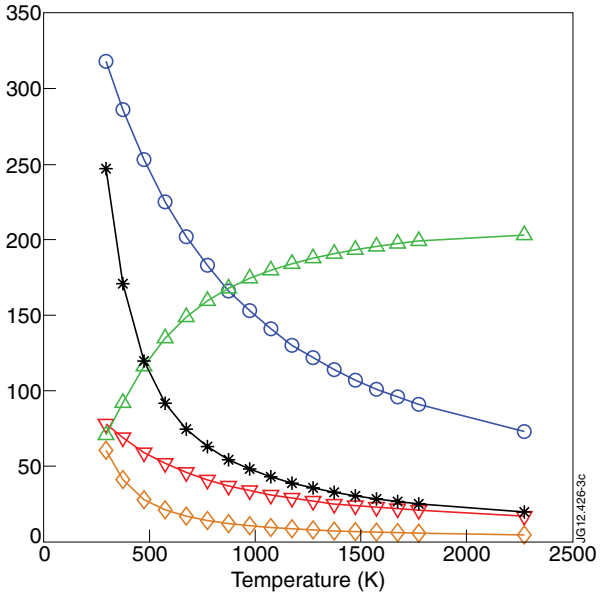

Figure 3: Evolution the thermal properties of the CFC dunlop. (− o −) z thermal conductivity in the direction z (depth) ($W.m^{-1}.K^{-1}$). (− ▽ −) x thermal conductivity in the direction x (poloidal) ($W.m^{-1}.K^{-1}$). (− △ −) specific heat capacity($\times 10^{-1}$ ($J.kg^{-1}.K^{-1}$)). (−∗−) thermal diffusivity ($\times 10^{6}$ ($m^2.s^{-1}$)) in the direction z (depth). (−◇−) thermal diffusivity $\times 10^{6}$ ($m^2.s^{-1}$)) in the direction x (poloidal).

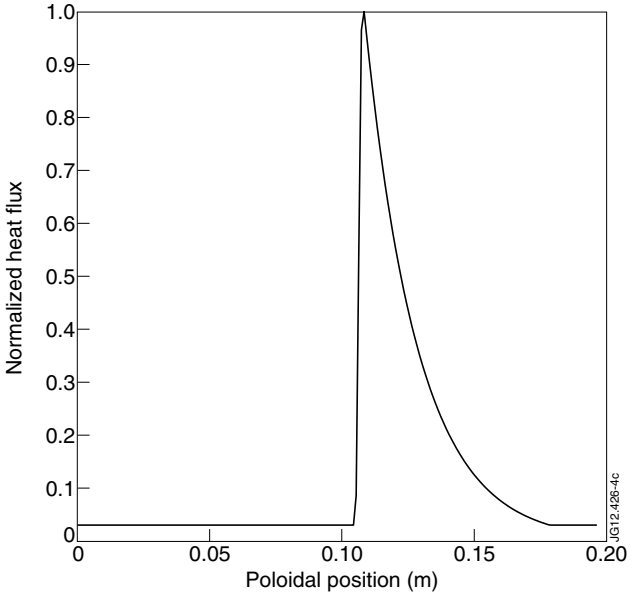

Figure 4: Normalized 'a priori' shape function '(x) of the spatial heat flux distribution.

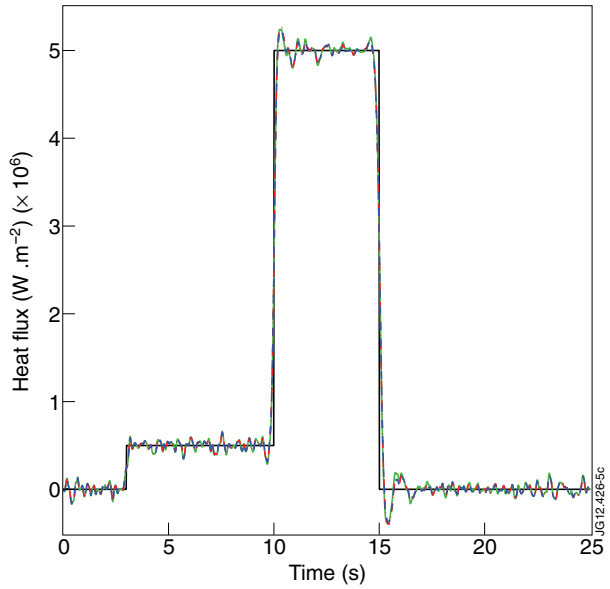

Figure 5: Evolution of the maximal heat flux (t) versus time with noisy data noise = 0.5K. (—) exact evolution of (t). Estimated evolution of (t) with different modelling: (– –) radiative exchange equal to "cfc on all boundaries, (– –) radiative exchange equal to "cfc on Γ_1 and "w on Γ_2, (– –) radiative exchange and W coating modelling.

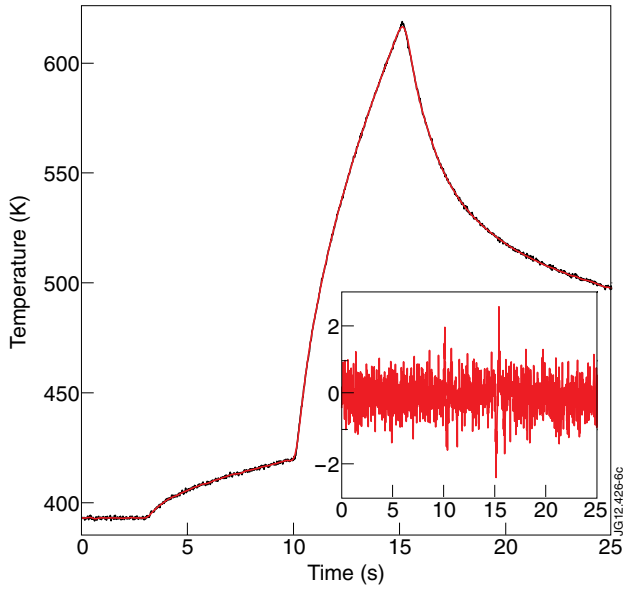

Figure 6: Evolution of the temperature at the TC location versus time. (—) noisy data with noise = 0.5K. (—) recovered temperature with estimated ϕ (x, t). The insert shows the residuals between noisy data and recovered temperature.

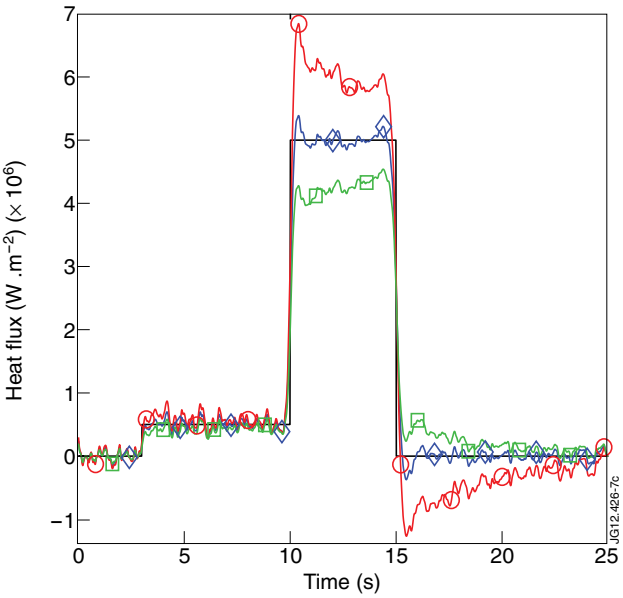

Figure 7: Evolution of the maximal heat flux $\phi(t)$ versus time. (—) exact evolution of $\phi(t)$. Estimated evolution of (t) with noisy data σ_{noise} = 0.5K and different location of the strike point: (– ◇ –) exact position, (– ○ –) error of −0.5cm, (– □ –) error of +0.5cm.

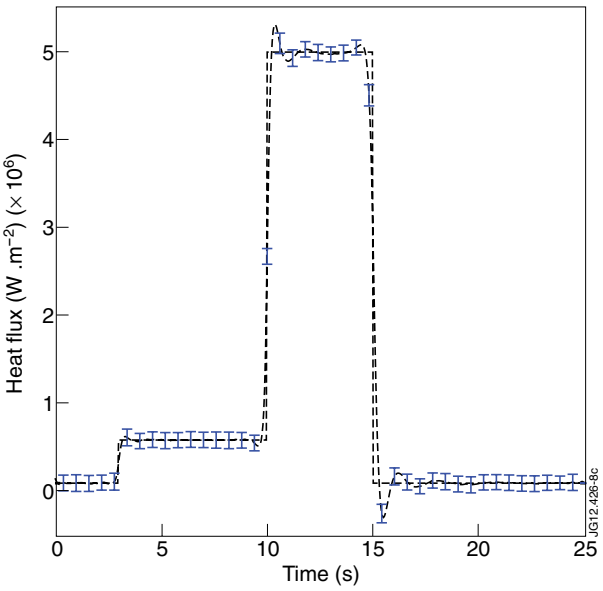

Figure 8: Evolution of the maximal heat flux $\phi(t)$ versus time. (- - -) exact evolution of $\phi(t)$. (—) average of all Monte Carlo estimation of $\phi(t)$ with the 68% confidence interval for noise = 0.5K.

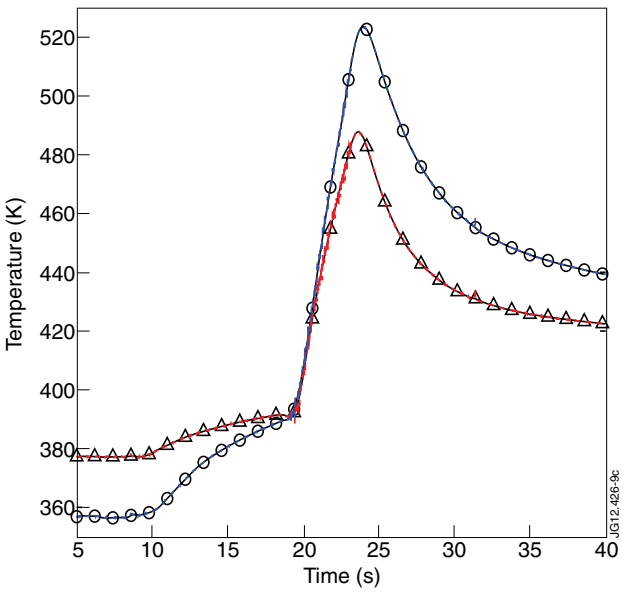

Figure 9: Upper thermocouples measurements for the Pulse No: 82641: (- - -) tile 3, (- - -) tile 7. Recovered temperature with estimated $\phi(x,t)$: (– △ –) tile 3, (– ○ –) tile 7.

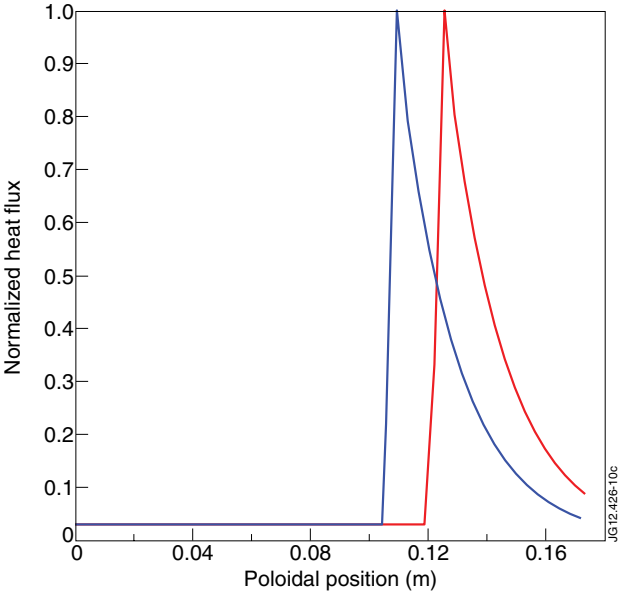

Figure 10: Normalized 'a priori' shape function of the spatial heat flux distribution. (—) tile 3 (inner). (—) tile 7 (outer).

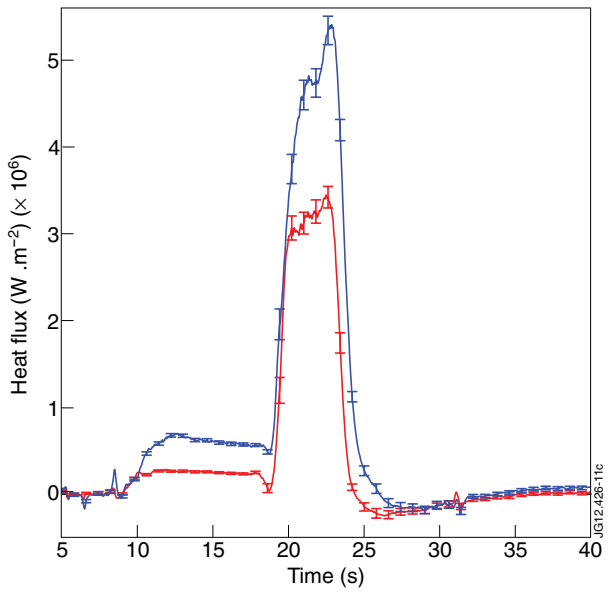

Figure 11: Evolution of the estimated maximal heat flux $\phi(t)$ versus time with upper thermocouples measurements on tiles 3 and 7. (—) estimated evolution of $\phi(t)$ on tile 3 with the 68% confidence interval for the measurement noise. (—) estimated evolution of $\phi(t)$ on tile 7 with the 68% confidence interval for the measurement noise.

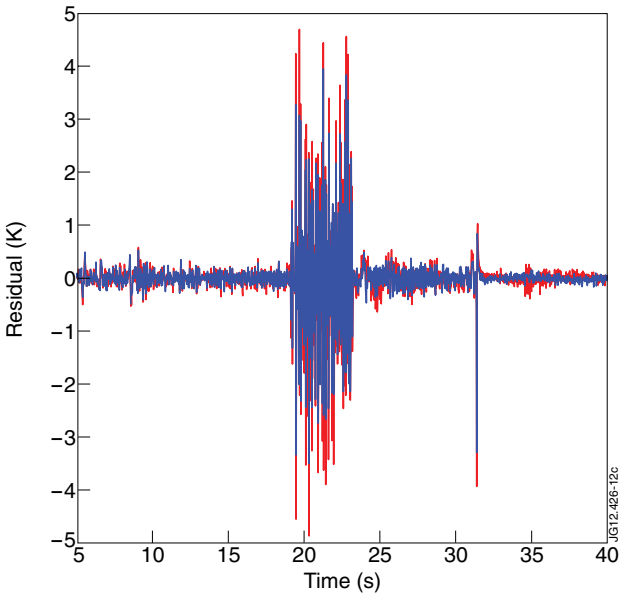

Figure 12: Residuals between upper thermocouples measurements and recovered temperature: (—) tile 3, (—) tile 7.

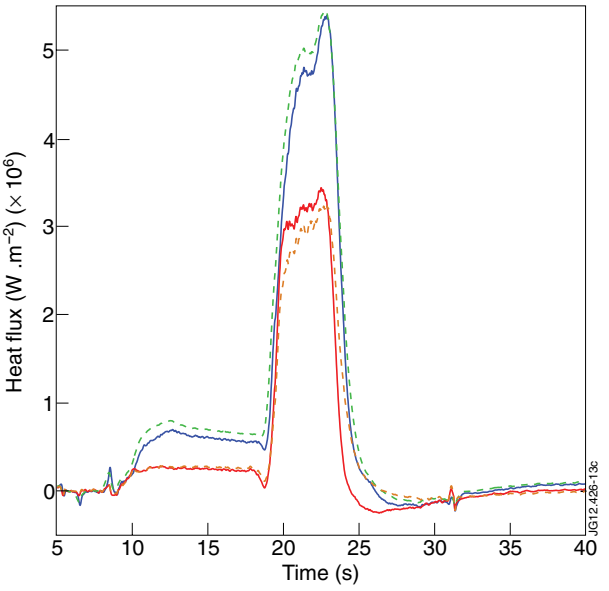

Figure 13: Evolution of the estimated maximal heat flux (t) versus time with upper thermocouples measurements on tiles 3 and 7 for the Pulse No:82641. (—) estimated evolution of (t) on tile 3 with the CGM. (—) estimated evolution of (t) on tile 7 with the CGM. (- - -) estimated evolution of (t) on tile 3 with linear approach. (- - -) estimated evolution of (t) on tile 7 with linear approach.